polysaccharides

MDPI

Article

Impact of Molecular Weight on the Permeation Enhancement and Barrier Interaction of Fucoidan as a Transdermal Delivery Candidate

Jialing Wu [1,2], Meiyue Zhao [1,2], Huaide Liu [3], Lihua Geng [1,4], Ning Wu [1,4], Yang Yue [1,4], Xiuliang Wang [1,4], Quanbin Zhang [1,4], Sara A. Cunha [5], Manuela Pintado [5] and Jing Wang [1,4,*]

1 Laboratory of Experimental Marine Biology, Institute of Oceanology, Chinese Academy of Sciences, Qingdao 266000, China; ujial1103@163.com (J.W.)
2 University of Chinese Academy of Sciences, Beijing 100049, China
3 Department of Science, Xinglin College, Nantong University, Qidong Campus, Nantong 226019, China
4 Laboratory for Marine Biology and Biotechnology, Qingdao Marine Science and Technology Center, Qingdao 266237, China
5 CBQF—Centro de Biotecnologia e Química Fina, Laboratório Associado, Escola Superior de Biotecnologia, Universidade Católica Portuguesa, Rua Diogo Botelho 1327, 4169-005 Porto, Portugal
* Correspondence: jingwang@qdio.ac.cn; Tel.: +86-532-82898703

Abstract

Fucoidan (FPS), a sulfated polysaccharide isolated from brown algae with a molecular weight ranging approximately from 5 to 200 kDa, exhibits diverse bioactivities, yet its high molecular weight (HMW) restricts topical bioavailability. This study explored the molecular-weight-dependent transdermal behavior of FPS and its underlying interaction mechanisms with the skin barrier. To address this, FPS fractions (6 to 103 kDa) were prepared via controlled oxidative degradation. In vitro permeation studies combined with Confocal Laser Scanning Microscopy (CLSM) visualization revealed a critical molecular weight threshold of approximately 11 kDa. HMW-FPS were mainly retained on the skin surface, whereas low molecular weight FPS (LMW-FPS, ≤11 kDa) penetrated into the viable epidermis and dermis. ATR-FTIR spectroscopy was employed to elucidate the underlying mechanism, which revealed that LMW-FPS overcomes the skin barrier through synergistic structural modulations: (1) it enhances intercellular lipid fluidity, accompanied by a reduction in CH_2 stretching vibration intensity; (2) it induces conformational changes in keratin via direct electrostatic interactions, promoting the transition from α-helices to β-sheets. Furthermore, histological evaluation confirmed that FPS treatment caused no obvious skin irritation. These findings demonstrate that LMW-FPS acts as a safe, reversible modulator of the stratum corneum (SC) barrier, providing a promising strategy for the design of polysaccharide-based transdermal delivery systems.

Keywords: fucoidan; various molecular weights; transdermal penetration; stratum corneum barrier; cosmetic biomaterials

Academic Editor: Gloria Huerta-Angeles

Received: 9 April 2026
Revised: 30 May 2026
Accepted: 2 June 2026
Published: 4 June 2026

1. Introduction

As the body's largest organ and primary physical barrier, skin is structurally organized into the epidermis, dermis and subcutaneous tissue [1]. Its protective barrier function is primarily attributed to the SC, the outermost layer of the epidermis. This layer features a compact microstructure; closely packed corneocytes are embedded within organized intercellular lipids, constructing a robust protective barrier that blocks penetration and invasion

of external substances [2,3]. However, this formidable defensive barrier also presents a significant challenge for dermatological therapy and cosmeceuticals, as it severely limits the percutaneous penetration of hydrophilic bioactive ingredients into the deeper viable layers. Despite these barriers, there is a growing scientific interest in exploiting natural biopolymers for transdermal applications. Existing studies have clearly demonstrated that molecular weight is one of the core factors regulating the transdermal absorption efficacy of hydrophilic macromolecules. For instance, despite its name, hyaluronic acid (HA) is essentially a polymer. Studies have shown that its interaction with the SC exhibits obvious molecular size dependence, and LMW fractions possess superior skin penetration [4–6]. Similarly, the structure–activity relationships of other polysaccharides (e.g., heparin, galactomannan and dextran) further confirm that LMW fractions generally possess enhanced bioactivity and skin permeation properties [7–10].

Fucoidan is a prominent sulfated polysaccharide derived from brown algae cell walls, and possesses diverse structures linked to a wide range of biological activities relevant to skin health [11]. Its characteristic structure consists primarily of fucose units connected via α-l-(1 → 4) and α-l-(1 → 3) glycosidic bonds, with sulfate groups typically esterified at positions C-2, C-3, and/or C-4 [12]. Depending on the algal source and extraction method, the molecular weight of FPS varies considerably, ranging from approximately 5 kDa to over 200 kDa [13]. Research has confirmed that FPS exhibits superior properties suitable for dermal cosmetic applications, including prominent moisture retention, antibacterial activity, strong antioxidant capacity, inhibitory effects on melanin synthesis, and anti-photoprotection against UV irradiation [14–16]. Combined with its favorable biocompatibility, these characteristics render FPS a promising functional ingredient for skincare and topical dermatological therapy.

However, a critical determinant governing topical bioavailability is the capacity of cosmetic and therapeutic agents such as FPS to penetrate the skin barrier and reach the targeted active sites. Although the inherent hydrophilicity and macromolecular structure of polysaccharides theoretically restrict SC permeation, inconsistent experimental observations have been reported. Several investigations have confirmed that FPS is capable of skin penetration; for example, Pozharitskaya et al. verified the effective transdermal delivery of FPS across rat skin into underlying cutaneous tissues and systemic circulation, particularly upon combination with essential oils [17]. Similarly, Barbosa et al. reported significantly enhanced skin permeability coefficients for FPS/alginate formulations incorporated with essential oil components [18]. Mechanistically, FPS may interact with SC keratin via hydrogen bonding, thereby modulating skin barrier integrity, promoting transdermal permeation, and ameliorating cutaneous physiological status [19,20]. Notably, our prior related work demonstrated that FPS fractions with varying molecular weights exhibit superior hygroscopicity and moisturizing capacity compared with HA, highlighting their potential as innovative raw materials for dermal cosmetic systems [21]. It should be noted that strong hygroscopicity will not impair the moisturizing performance of the material. Instead, it efficiently absorbs ambient moisture to supply sufficient water and further improve skin hydration. Nevertheless, these studies often involve complex formulations, and the specific role of molecular weight in the intrinsic permeation behavior of FPS, along with the molecular-level mechanisms of its interaction with skin lipids and proteins, remains insufficiently elucidated. Therefore, this study aims to systematically investigate the influence of molecular weights on the transdermal penetration and retention mechanisms of FPS. We prepared FITC-labeled FPS fractions with defined molecular weight ranges (6–103 kDa) to visually assess their penetration depth and distribution within ex vivo pig skin using CLSM. Furthermore, the specific interactions between FPS and skin components (lipids and keratin) were probed using Attenuated Total Reflectance Fourier Trans-

form Infrared spectroscopy (ATR-FTIR), complemented by histological safety evaluations (H&E staining). The insights gained aim to clarify the structure-permeability relationships of sulfated polysaccharides, providing a theoretical foundation for developing LMW-FPS as a functional carrier or enhancer in novel transdermal formulations.

2. Materials and Methods

2.1. Materials

Saccharina japonica was collected from Rongcheng (Shandong, China). Hydrogen peroxide and ascorbic acid were purchased from Sinopharm Chemical Reagent Co., Ltd., Shanghai, China. Bama ex vivo pig skin (dorsal tissue) was purchased from Beijing Jixing Dacheng Technology Co., Ltd., Beijing, China. All other chemicals used in this study were of analytical grade.

2.2. Preparation of FPS with Different Molecular Weights via Oxidative Degradation

The raw material used was fucoidan (designated as F-4) extracted from *Saccharina japonica* in the laboratory. Briefly, dried seaweed was treated in high-temperature and high-pressure water at 115–125 °C (0.10–0.15 MPa) for 3–4 h, followed by filtration, dialysis, concentration, precipitation with 75% ethanol, and freeze-drying to obtain crude fucoidan [21]. To obtain fucoidan fractions of different molecular weights (F-1, F-2, and F-3), an oxidative degradation approach adapted from Li et al. [22] was employed, as outlined in Table 1. Briefly, F-4 was completely dissolved in water at specific temperatures (60 °C, 80 °C, or 100 °C) under continuous stirring to prepare a 2% (*w*/*v*) stock solution. Hydrogen peroxide and ascorbic acid were then added in a 1:1 volume ratio to final concentrations of 5 mM, 20 mM or 30 mM, while adjusting the final sugar concentration to 1% (*w*/*v*). After the reaction was complete, the liquid degradation products were then desalted using dialysis membranes (F-2 and F-3, MWCO: 3.5 kDa) and Sephadex G-10 gel filtration chromatography (F-1), followed by lyophilization to obtain solid FPS samples. Finally, the physicochemical properties of the resulting fractions were characterized to confirm the consistency and stability of the preparation process.

Table 1. The preparation parameters of degraded FPS.

Samples	Temperature/°C	Final Oxidant Concentration/mM	Time/h
F-1	100	30	4
F-2	80	20	1
F-3	60	5	2

2.3. Analysis of Physicochemical Properties

Fucose content was determined via the cysteine hydrochloride method using L-fucose as the standard [23], while sulfate content was measured by the gelatin-$BaCl_2$ method with potassium sulfate solution as the standard, adapted from Chen et al. [24]. Uronic acid content was analyzed through the carbazole colorimetric method with D-glucuronic acid as the standard [25]. The total sugar content was quantified using the sulfuric acid–phenol method with L-fucose as the standard [26]. Additionally, molecular weight was assayed using an HP-GPC system [27].

2.4. Interaction Between FPS with Different Molecular Weights and the Skin

2.4.1. Determination of Skin Distribution of FITC-FPS

The distribution profile of FPS with different molecular weights within skin tissue was assessed using fluorescein isothiocyanate (FITC)-labeled polysaccharides. The method for FITC labeling of the polysaccharides was performed according to the protocol described by

Yu-Hao et al. [28], with minor revisions. Vertical Franz diffusion cells were employed for this analysis. Ex vivo pig skin was mounted in the diffusion cells with SC facing the donor compartment and dermis contacting the receptor compartment filled with 3 mL PBS buffer (pH 7.4). The assembly was maintained at 32 ± 0.5 °C with receptor solution stirred at 400 rpm. Subsequently, 1 mL of FITC-FPS solution was applied to the donor compartment. Skin samples were harvested at predetermined intervals (1, 4, 12, and 24 h), rinsed with normal saline, and surface-dried with filter paper. Each sample was then embedded in OCT compound, flash-frozen in liquid nitrogen, and cryosectioned. Transverse sections (thickness: 10 μm) were mounted on glass slides for visualization of FITC fluorescence distribution across skin layers using CLSM (Olympus, Shinjuku City, Japan).

2.4.2. ATR-FTIR Measurement

The molecular interactions between FPS fractions and key skin barrier components were investigated using ATR-FTIR spectroscopy (Thermo Fisher Scientific, Waltham, MA, USA), focusing on hydration state, keratin conformation, and lipid organization. SC membranes were prepared by incubating porcine skin sections (0.25 cm^2) dermal-side down in 24-well plates containing PBS (pH 7.4) with 0.2% trypsin at 37 °C for 8 h to separate the epidermis. After enzymatic treatment, the SC was gently separated from underlying tissue, washed thoroughly with deionized water, and vacuum-desiccated for 24 h. Dried SC membranes were then immersed in either 3 mL normal saline (control) or 3 mL of 1% (*w*/*v*) FPS solutions (various molecular weights) within 6-well plates for 12 h at room temperature. Following incubation, membranes were rinsed three times with distilled water and vacuum-desiccated (silica gel) for 12 h. ATR-FTIR spectra were acquired with the following parameters: resolution of 2 cm^{-1}, number of scans of 100, and scanning range of 650–4000 cm^{-1}. The spectra were analyzed using Origin 2024 software (OriginLab, Northampton, MA, USA).

2.5. Hematoxylin–Eosin (H&E) Staining of Ex Vivo Pig Skin

Histological examination via H&E staining was performed to evaluate potential microstructural changes in porcine skin following exposure to FPS solutions. Skin samples, equilibrated at room temperature for 30 min after removal from −20 °C storage, were treated with 100 μL of 1% (*w*/*v*) FPS solution (experimental groups) or left untreated (control). Both groups were incubated under identical conditions for 1, 4, 8, and 24 h. After treatment, specimens were embedded in OCT medium, snap-frozen in liquid nitrogen, and stored at −20 °C until sectioning. The specific staining procedure was as follows: Cryosections (5–7 μm thickness) were affixed on glass slides and stained following the standard H&E protocol: stained with hematoxylin (2 min), rinsed with water (5–10 s), placed in differentiation solution (3 s), thoroughly rinsed with tap water (2 min), counterstained with eosin (3 s) and finally rinsed with tap water (1 min). The stained tissue images were visualized under a microscope (Olympus, Shinjuku City, Japan).

3. Results

3.1. Chemical Analysis

Fucoidan extracted from *Saccharina japonica* in the laboratory (designated as F-4) was used as the raw material. Three degraded samples (F-1, F-2, and F-3) with different molecular weights were obtained under various experimental conditions. To elucidate the influences of degradation modification on the chemical profiles of FPS, systematic characterization and comparative analysis of physicochemical properties were performed across the four fractions. As summarized in Table 2, polysaccharide fractions exhibited a well-defined gradient distribution in molecular weight after stepwise degradation, ranging

from 6 kDa to 103 kDa (Supplementary Figure S1). Total carbohydrate contents fluctuated slightly from 55.62% to 56.57%. Uronic acid levels remained relatively low throughout all samples (2.04–7.26%), and no significant linear correlation was identified between uronic acid content and molecular mass. As the predominant characteristic monosaccharide of FPS, fucose constituted the major component in all tested fractions, accounting for 25.15–29.75% of the total mass. In addition, sulfate groups, as critical structural moieties closely associated with biological bioactivity, were detected at contents of 23.44–25.72%. Although minor variations in total carbohydrate and sulfate contents were observed during degradation, no pronounced loss of typical functional groups occurred in the overall structural framework.

Table 2. The chemical composition of FPS with different molecular weights.

Samples	Fucose (%)	Sulfate (%)	Uronic Acid (%)	Total Sugar (%)	Molecular Weight (kDa)
F-1	26.16 ± 0.38	24.57 ± 1.12	2.44 ± 0.05	58.81 ± 1.32	6.10
F-2	27.55 ± 0.20	25.72 ± 0.82	2.04 ± 0.16	57.61 ± 1.57	11.10
F-3	27.71 ± 0.04	23.44 ± 0.35	2.26 ± 0.47	56.57 ± 0.33	33.70
F-4	29.75 ± 0.35	25.63 ± 0.43	2.64 ± 0.05	55.62 ± 0.95	103.25

Data shown represent mean ± standard deviation.

3.2. Interaction Results of Different Molecular Weights with Skin

3.2.1. CLSM Analysis of FITC-FPS Distribution in Ex Vivo Pig Skin with Different Molecular Weights

FITC-FPS samples with different molecular weights were applied to ex vivo pig skin, and their transdermal profiles were observed via CLSM. As shown in Figure 1, free FITC served as the control group; its molecules diffused throughout skin tissues within 4 h and gradually accumulated predominantly around hair follicles (outlined in red circles). All FITC-FPS conjugates initially adhered to the SC surface (pointed by yellow arrows). However, only F-1 and F-2 demonstrated progressive penetration through the SC barrier into the dermis. The fluorescent signals of F-1 and F-2 were first detected in the dermis at 4 h, peaked between 4 h and 12 h, and remained clearly detectable at 24 h, indicating sustained dermal retention. In contrast, F-3 showed delayed penetration, with dermal fluorescence first observed at 12 h. Although signal intensity gradually increased during the 12–24 h period, it remained substantially weaker than that of F-1 and F-2. F-4 exhibited negligible dermal penetration, with fluorescence persistently concentrated on the SC surface throughout the 24 h observation period and no measurable signal detected in deeper tissues. These findings demonstrate that molecular weight critically influences the transdermal penetration of FPS. LMW-FPS ($\leq$11 kDa) efficiently crossed the skin barrier, achieving significant dermal accumulation and prolonged retention ($\geq$24 h), likely facilitated by specific interactions with SC components that enable penetration without permanent structural disruption. This sustained dermal presence suggests their potential utility as carriers in transdermal drug delivery systems. By contrast, HMW-FPS (>11 kDa) remained largely confined to the SC surface, exhibiting minimal penetration capability.

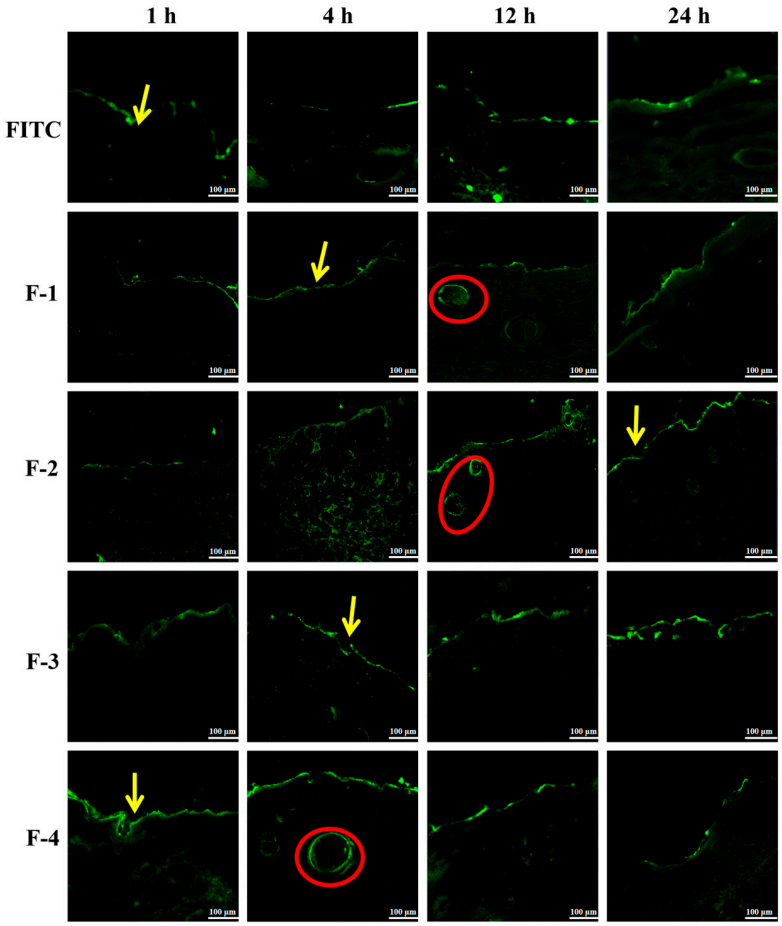

Figure 1. Confocal laser imaging of different molecular weights FPS-FITC in ex vivo pig skin (scale bar: 100 μm). Note: FITC is shown in green, the yellow arrow refers to the SC layer, and hair follicles are outlined in red circles.

3.2.2. ATR-FTIR Analysis/Interaction with Skin Barrier

1. Interaction with skin keratin

ATR-FTIR spectroscopy was employed to investigate molecular interactions between FPS and skin barrier components, with particular focus on conformational changes of keratin in the SC. This technique monitors changes in molecular vibrations, whereby shifts in characteristic absorption peaks reflect structural alterations in keratin—a dominant SC protein accounting for 75–80% of its composition [29]. Changes in keratin's secondary structure were monitored using the amide I (≈1640 cm^{-1}) and amide II (≈1540 cm^{-1}) bands, which are established markers of protein conformation [30]. As shown in Figure 2 (dashed box), the absorption peaks correspond to keratin vibrational modes in the SC. Control samples treated with normal saline exhibited amide I and II peaks at 1643.78 cm^{-1} and 1537.25 cm^{-1}, respectively. Treatment with 1% FPS solutions induced notable blueshifts in these peaks. F-1 and F-2 produced the most significant displacements: F-1 caused a maximum amide I blueshift of 2 cm^{-1}, while F-2 resulted in the largest amide II shift of 6 cm^{-1}. In contrast, F-3 and F-4 induced considerably smaller peak shifts.

These spectral alterations indicate molecular weight-dependent interactions between FPS and keratin. The observed blueshifts suggest structural transitions in keratin's secondary structure, characterized by an increase in β-sheet and random coil conformations relative to α-helix. The magnitude of peak displacement exhibited an inverse correlation with FPS molecular weight, pointing to stronger keratin interactions with LMW fractions such as F-1 and F-2.

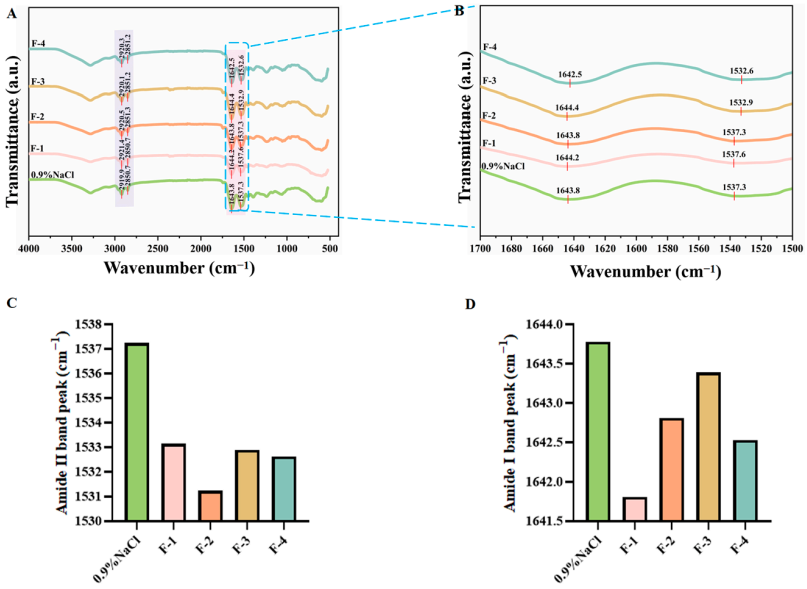

Figure 2. Effects of 0.9% NaCl and different molecular weights FPS on vibrational peak shift of SC keratin in ex vivo pig skin. (**A**) Full-range FTIR spectra. (**B**) Magnified view of the amide I and amide II bands. (**C**) Comparison of amide II band peak positions. (**D**) Comparison of amide I band peak positions.

2. Interaction with skin lipids

ATR-FTIR spectroscopy was further employed to examine interactions between FPS and SC lipids, which constitute 5–15% of the SC and critically maintain barrier integrity by limiting transepidermal water loss and blocking exogenous threats [31,32]. Lipid organization was evaluated through symmetric (≈2850 cm^{-1}) and asymmetric (≈2920 cm^{-1}) C–H stretching vibrations of methylene groups in alkyl chains, where peak shifts reflect changes in lipid packing density and fluidity [33,34]. As shown in Figure 3, control samples treated with normal saline displayed characteristic peaks at 2850.72 cm^{-1} and 2919.92 cm^{-1}. Application of 1% FPS solutions induced slight but consistent redshifts in both C–H vibration bands across all treatment groups.

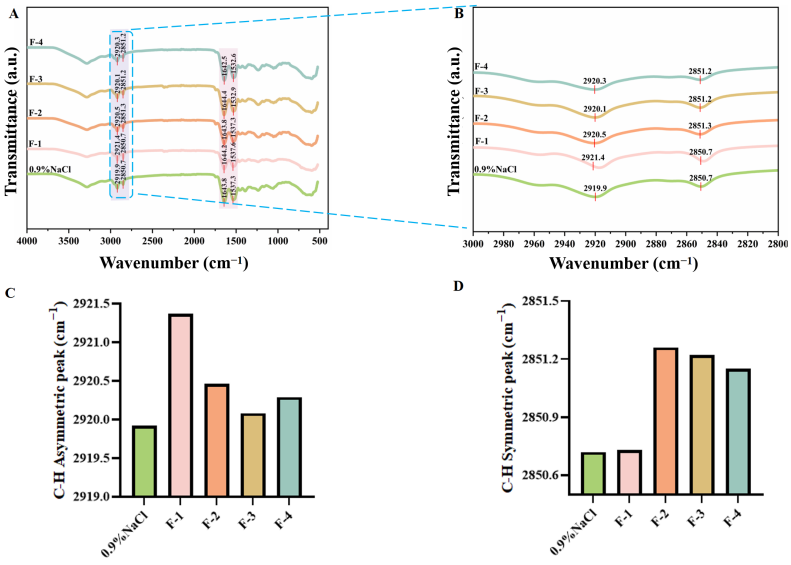

Figure 3. Effects of 0.9% NaCl and different molecular weights FPS on vibrational peak shift of SC lipid in ex vivo pig skin. (**A**) Full-range FTIR spectra. (**B**) Magnified view of the C–H stretching region. (**C**) Comparison of asymmetric C–H stretching peak positions. (**D**) Comparison of symmetric C–H stretching peak positions.

These spectral shifts indicate a transition from ordered trans conformations to disordered gauche conformations within lipid alkyl chains, signifying increased molecular mobility and reduced structural order in the lipid lamellae. The observed changes suggest weak yet specific interactions between FPS molecules and SC lipids that transiently disrupt bilayer organization. Importantly, LMW-FPS (≤11 kDa), particularly fraction F-1, induced more pronounced effects compared with HMW-FPS (>11 kDa) counterparts. This molecular-weight-dependent disruption synergizes with spectral shifts in keratin bands, including blue shifts of $\Delta 2$ cm^{-1} for amide I and $\Delta 6$ cm^{-1} for amide II (Section 3.2.2. 1. Interaction with skin keratin), collectively enhancing lipid fluidity and compromising the barrier's structural coherence. The resultant increase in SC permeability provides a mechanistic basis for the enhanced transdermal penetration of LMW-FPS documented in CLSM studies.

3.3. H&E Staining of Ex Vivo Pig Skin

H&E staining of ex vivo pig skin treated with 1% FPS solutions showed structural changes limited exclusively to the SC, with clear dependence on treatment time and FPS molecular weight. As shown in Figure 4, saline-treated control skin maintained a continuous, compact SC layer over 24 h, with only slight surface loosening and intact dermal collagen. In contrast, FPS treatment induced SC swelling and separation from the viable epidermis, driven by increased hydration. These changes peaked at 4–8 h and were most prominent for LMW-FPS (F-1 and F-2, ≤11 kDa), which caused marked interlayer expansion and partial detachment. F-3 induced milder separation, while F-4 showed negligible changes. Importantly, these structural alterations were confined to the SC and had no destructive impact on other skin layers. By 24 h, the SC largely recovered its normal architecture, confirming that the modifications were transient and reversible.

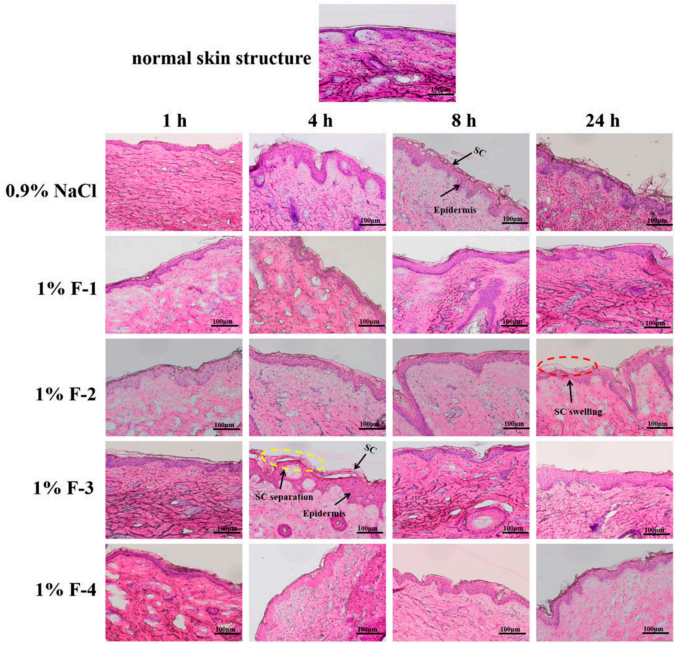

Figure 4. H&E staining of ex vivo pig skin treated with FPS solutions of different molecular weights at different times (scale bar: 100 μm). Note: yellow dotted circles denote SC separation, red dotted circles denote SC swelling, and arrows point to the SC and epidermis, respectively.

4. Discussion

SC serves as the primary rate-limiting barrier restricting the transdermal delivery of exogenous bioactive molecules. Molecular weight is a critical governing factor modulating skin permeation behavior, as widely documented for HA. LMW-HA (≤10 kDa) exhibits

superior transdermal penetration relative to HMW-HA, facilitating its deeper deposition within the dermis via specific interactions with skin barrier components [5,6]. Similarly, Farwick et al. confirmed that oligosaccharide HA fractions exhibit potent skin penetration activity [4]. Despite exhibiting multiple beneficial bioactivities including moisture retention, melanin inhibition, photoprotection and antioxidant capacity as a topical skincare agent, the transdermal permeation mechanism of FPS and the regulatory contribution of molecular weight remain poorly and systematically elucidated. This study addresses this critical research gap, providing systematic evidence illustrating the molecular-weight-dependent transdermal permeation enhancement of FPS, alongside confirming its satisfactory biocompatibility and unique barrier-interaction mechanisms.

To validate these properties under physiologically relevant conditions, we evaluated the permeation of FPS using ex vivo pig skin, a validated model with structural and compositional similarity to human skin [35,36]. CLSM tracking revealed critical molecular-weight-dependent divergence: LMW-FPS ($\leq$11 kDa) rapidly penetrated the SC within 4 h, progressively accumulating in deeper tissues with sustained retention (>24 h). Conversely, HMW-FPS (>11 kDa) showed delayed or negligible penetration, remaining largely confined to the superficial SC. This pattern aligns with findings for HA, where fractions below 8 kDa permeate effectively while larger chains accumulate superficially [6,37]. Furthermore, the intense fluorescence signals observed in hair follicles indicate that LMW-FPS utilizes the follicular pathway as a significant shunt route. This observation confirms that the appendageal route complements the primary intercellular pathway, consistent with the established penetration behavior of hydrophilic macromolecules [38,39]. This molecular-weight-dependent permeation profile likely arises from structural and rheological differences: LMW-FPS possesses shorter chains and lower viscosity, enabling rapid penetration across the SC with minimal steric hindrance and efficient accumulation in the viable epidermis and dermis. In contrast, HMW-FPS features longer chains and higher viscosity, readily adsorbing to surface lipids and being restricted to the SC by combined steric hindrance and viscous resistance.

Transdermal penetration through the SC is dominated by passive transport, including intercellular lipid diffusion and appendageal pathways [40]. Consistent with our CLSM observations, the hair follicle route acts as a critical shortcut for FPS delivery. Energy-dependent active processes, such as endocytosis and pinocytosis, mainly contribute to cellular uptake in viable epidermal and dermal cells after SC penetration, rather than participating in the initial barrier traversal.

Given these macroscopic disparities in penetration depth and distribution, we employed ATR-FTIR spectroscopy to interrogate the underlying molecular interactions responsible for overcoming the barrier. Our analysis suggests that the enhanced permeation of LMW-FPS arises from three interconnected mechanisms targeting specific SC components. Initially, LMW-FPS ($\leq$11 kDa) significantly enhances SC hydration, a process that reversibly disrupts intercorneocyte junctions and the organization of lipid lamellae, thereby creating a more permeable environment. Concurrent with hydration, LMW-FPS markedly induces conformational rearrangement of keratin. The negatively charged sulfate groups in LMW-FPS establish specific electrostatic interactions with the amino acid residues of SC keratin. Unlike HMW chains, which are restricted to surface adsorption due to significant steric hindrance, the reduced hydrodynamic radius of LMW-FPS grants it superior accessibility to the internal binding sites within the keratin matrix. This accessibility allows LMW-FPS to deeply penetrate and disrupt the intramolecular and intermolecular hydrogen-bonding networks of keratin, promoting the disassembly of compact α-helical and their transition into looser β-sheets and random coils. The amide I band at $\approx$1640 cm^{-1} is assigned to the C=O stretching vibration of peptide bonds, while the amide II band at $\approx$1540 cm^{-1} corresponds

to N–H bending coupled with C–N stretching vibration [30,41]. Such secondary structural transformation is supported by distinct blue shifts of the amide bands, with a shift of $\Delta 2$ cm^{-1} for amide I and $\Delta 6$ cm^{-1} for amide II. Reorganization of the keratin secondary structure further opens the intracellular polar pathway, attenuating charge repulsion and steric hindrance of the skin barrier. Consequently, LMW-FPS enhances bilayer fluidity and expands molecular diffusion pathways much more effectively than its HMW counterparts.

In addition to protein modulation, LMW-FPS actively disrupts the ordered arrangement of the SC lipid bilayer. This effect is strictly governed by molecular size: while HMW-FPS is largely excluded from the dense lipid lattice, LMW chains are sufficiently compact to physically intercalate into the lipid bilayer. Once inserted, the hydroxyl and sulfate groups form dynamic hydrogen bonds with the polar headgroups of lipids, while the hydrophobic fucose backbone intercalates into the lipid alkyl chain region, disrupting the cross-linked network between lipid molecules. Simultaneously, the hydrophobic fucose backbone intercalates into the lipid alkyl chain packing region, weakening van der Waals forces and hydrophobic association between alkyl chains. The symmetric ($\approx$2850 cm^{-1}) and asymmetric ($\approx$2920 cm^{-1}) C–H stretching vibrations are characteristic of alkyl chains in SC lipids, widely used to evaluate lipid packing and fluidity [33,34,42]. The observed redshift in these bands reflects a transition from ordered trans to disordered gauche conformations, indicating lipid fluidization and increased bilayer permeability [43]. Notably, although the FTIR instrument had a nominal resolution of 2 cm^{-1}, its wavenumber precision (calibrated by an internal He–Ne laser) is better than $\pm$0.01 cm^{-1}. Thus, 1–2 cm^{-1} peak shifts exceed instrumental noise and reflect genuine physical changes, not measurement variability. Such subtle shifts are widely accepted as valid evidence for lipid rearrangement in transdermal research. For example, hyaluronic acid studies have reported meaningful lipid peak shifts of only 0.2–0.8 cm^{-1} [6]. And flavonoid transdermal research considered a 1 cm^{-1} shift as sufficient to indicate lipid disordering [41]. Consistently, the 1–2 cm^{-1} shifts observed here represent genuine changes in lipid packing induced by FPS [42]. Consequently, LMW-FPS enhances bilayer fluidity and expands molecular diffusion pathways much more effectively than its HMW counterparts. While polysaccharides like LMW-HA and chitosan also modulate lipids via hydrogen bonding or electrostatic interactions, FPS appears to offer a unique advantage due to its sulfated modification. Beyond molecular weight, sulfate groups are key functional moieties driving the barrier-modulating activity of FPS. Their strong negative charge mediates electrostatic attraction to keratin, promoting structural rearrangement; their high polarity strengthens hydrogen bonding with lipid headgroups, increasing bilayer fluidity. These sulfate-driven interactions are more pronounced in LMW-FPS, as smaller molecular size reduces steric hindrance and allows deeper access to SC components. Together, molecular weight and sulfate substitution act synergistically to determine the superior transdermal performance of LMW-FPS [6,44–46]. Importantly, despite these structural modulations, histological analysis confirmed that all FPS fractions maintained tissue biocompatibility without causing inflammation or irreversible damage. This confirms that the barrier modulation by LMW-FPS is transient and safe.

Collectively, our findings demonstrate that LMW-FPS ($\leq$11 kDa) enhances transdermal permeation through a synergistic, multi-target mechanism. Hydration swells the SC structure, while sulfate-mediated electrostatic interactions drive keratin rearrangement to reduce protein barrier resistance. Simultaneously, hydrophobic intercalation and hydrogen bonding drive lipid fluidization to expand intercellular diffusion space, with the follicular route serving as an auxiliary channel. In contrast, HMW-FPS is limited by steric hindrance and high viscosity, preventing deep structural perturbation. Building upon these insights, this work establishes LMW-FPS as a potent, biosafe transdermal enhancer and a promising multifunctional carrier for pharmaceutical and cosmetic applications.

Future research directions arising from this study are proposed as follows. First, in vivo human trials should be conducted to systematically validate the transdermal behavior, skin tolerance, and safety profile of LMW-FPS, because human skin differs significantly from porcine skin in metabolic activity, immune responses, and barrier microstructure. Such trials will provide more clinically relevant evidence for its topical applications. Second, further investigations are warranted to explore the potential of LMW-FPS as a functional carrier for hydrophobic drugs. It is critical to evaluate the loading capacity, encapsulation efficiency, in vitro release kinetics, and skin permeation performance of LMW-FPS-based delivery systems. These efforts will facilitate the development of advanced polysaccharide-derived transdermal formulations, thereby expanding the practical utility of LMW-FPS beyond its intrinsic penetration-enhancing activity.

5. Conclusions

Experimental evidence confirms that FPS transdermal absorption is strictly dependent on its molecular weight. LMW-FPS achieve superior transdermal absorption by overcoming SC barrier resistance through a tripartite mechanism. First, hydration-driven SC reorganization induces reversible corneodesmosome dissociation and lipid lamellae disruption. Second, keratin undergoes conformational shifts from α-helix to β-sheet/random coil structures, reducing protein-mediated diffusion resistance. Third, lipid fluidization expands intercellular pathways. This synergistic action enables rapid LMW-FPS permeation (<4 h) into viable epidermal/dermal layers with sustained retention, while HMW FPS exhibit minimal absorption due to steric exclusion. Critically, these processes occur without barrier deterioration, preserving SC integrity and biocompatibility throughout absorption. This intrinsic barrier-penetrating capability, coupled with inherent bioactive properties, positions LMW-FPS (<11 kDa) as a promising candidate for enhancing the topical efficacy of bioactive ingredients while maintaining physiological safety.

Supplementary Materials: The following supporting information can be downloaded at: https://www.mdpi.com/article/10.3390/polysaccharides7020065/s1, Figure S1: GPC profiles and molecular weight distribution of FPS fractions.

Author Contributions: Conceptualization, J.W. (Jialing Wu) and J.W. (Jing Wang); methodology, J.W. (Jialing Wu), M.Z., M.P. and S.A.C.; formal analysis, J.W. (Jialing Wu); investigation, J.W. (Jialing Wu), L.G. and Y.Y.; resources, J.W. (Jing Wang); data curation, J.W. (Jialing Wu) and M.Z.; writing—original draft preparation, J.W. (Jialing Wu); writing—review and editing, J.W. (Jialing Wu), S.A.C., M.P. and J.W. (Jing Wang); visualization, J.W. (Jialing Wu); supervision, N.W., X.W., Q.Z. and J.W. (Jing Wang); project administration, Q.Z. and J.W. (Jing Wang); funding acquisition, H.L. and X.W. All authors have read and agreed to the published version of the manuscript.

Funding: This research was funded by the National key R&D Program of China (2023YFE0106200) and the Nantong Natural Science Foundation (JC2024090).

Institutional Review Board Statement: Not applicable.

Data Availability Statement: The raw data supporting the conclusions of this article will be made available by the authors on request.

Conflicts of Interest: The authors declare no conflicts of interest.

Abbreviations

The following abbreviations are used in this manuscript:

FPS	Fucoidan
HMW	High molecular weight
LMW	Low molecular weight

CLSM	Confocal Laser Scanning Microscopy
SC	Stratum corneum
HA	Hyaluronic acid
ATR-FTIR	Attenuated Total Reflectance Fourier Transform Infrared spectroscopy
H&E	Hematoxylin–Eosin
FITC	Fluorescein isothiocyanate

References

1. Xia, Q.; Li, D.; Yu, T.; Zhu, J.; Zhu, D. In vivo skin optical clearing for improving imaging and light-induced therapy: A review. *J. Biomed. Opt.* **2023**, *28*, 060901. [CrossRef]
2. Bouwstra, J.A.; Nădăban, A.; Bras, W.; McCabe, C.; Bunge, A.; Gooris, G.S. The skin barrier: An extraordinary interface with an exceptional lipid organization. *Prog. Lipid Res.* **2023**, *92*, 101252. [CrossRef]
3. Elisabetta, E.; Claudio, N.; Maddalena, S.; Rita, C. Nanomedicines to treat skin pathologies with natural molecules. *Curr. Pharm. Des.* **2019**, *25*, 2323–2337. [CrossRef]
4. Farwick, M.; Gauglitz, G.; Pavicic, T.; Köhler, T.; Wegmann, M.; Schwach-Abdellaoui, K.; Malle, B.; Tarabin, V.; Schmitz, G.; Korting, H.C. Fifty-kDa hyaluronic acid upregulates some epidermal genes without changing TNF-α expression in reconstituted epidermis. *Ski. Pharmacol. Physiol.* **2011**, *24*, 210–217. [CrossRef] [PubMed]
5. Nashchekina, Y.A.; Raydan, M. Noninvasive penetration of 5 nm hyaluronic acid molecules across the epidermal barrier (in vitro) and its interaction with human skin cells. *Ski. Res. Technol.* **2018**, *24*, 129–134. [CrossRef] [PubMed]
6. Ni, C.; Zhang, Z.; Wang, Y.; Zhang, Z.; Guo, X.; Lv, H. Hyaluronic acid and HA-modified cationic liposomes for promoting skin penetration and retention. *J. Control. Release* **2023**, *357*, 432–443. [CrossRef]
7. Li, L.; Zhu, Y.; Feng, C.; Zhao, D.; Jiang, J. Germination-Inspired enzymatic degradation of guar galactomannan and its synergistic skincare effects with aloe polysaccharides. *ACS Sustain. Chem. Eng.* **2025**, *13*, 19709–19721. [CrossRef]
8. Jiang, H.; Li, J.; Luo, S.; Cui, C.; Luo, L.; Li, Y.; Liang, Z. Oat β-Glucooligosaccharides: Preparation, characterization, skin permeability, and photodamage repair for skincare applications. *Carbohydr. Res.* **2025**, *557*, 109648. [CrossRef]
9. Franzè, S.; Gennari, C.G.; Minghetti, P.; Cilurzo, F. Influence of chemical and structural features of low molecular weight heparins (LMWHs) on skin penetration. *Int. J. Pharm.* **2015**, *481*, 79–83. [CrossRef]
10. Bucay, V.; Gold, M.H.; Andriessen, A. Low molecular weight heparan sulfate containing facial skin care for reducing inflammation and restoring aged-skin homeostasis. *J. Cosmet. Dermatol.* **2020**, *19*, 1851–1856. [CrossRef] [PubMed]
11. Awanthi, M.G.G.; Umosa, M.; Yuguchi, Y.; Oku, H.; Kitahara, K.; Ito, M.; Tanaka, A.; Konishi, T. Fractionation and characterization of cell wall polysaccharides from the brown alga *Cladosiphon okamuranus*. *Carbohydr. Res.* **2023**, *523*, 108722. [CrossRef]
12. Lu, S.Y.; Zhou, T.; Shabbir, I.; Choi, J.; Kim, Y.H.; Park, M.; Aweya, J.J.; Tan, K.; Zhong, S.; Cheong, K.L. Marine algal polysaccharides: Multifunctional bioactive ingredients for cosmetic formulations. *Carbohydr. Polym.* **2025**, *353*, 123276. [CrossRef]
13. Chen, Q.; Kou, L.; Wang, F.; Wang, Y. Size-dependent whitening activity of enzyme-degraded fucoidan from *Laminaria japonica*. *Carbohydr. Polym.* **2019**, *225*, 115211. [CrossRef]
14. Ahsan, H. The significance of complex polysaccharides in personal care formulations. *J. Carbohydr. Chem.* **2019**, *38*, 213–233. [CrossRef]
15. Aslam, A.; Bahadar, A.; Liaquat, R.; Saleem, M.; Waqas, A.; Zwawi, M. Algae as an attractive source for cosmetics to counter environmental stress. *Sci. Total Environ.* **2021**, *772*, 144905. [CrossRef]
16. Shao, P.; Shao, J.; Han, L.; Lv, R.; Sun, P. Separation, preliminary characterization, and moisture-preserving activity of polysaccharides from *Ulva fasciata*. *Int. J. Biol. Macromol.* **2015**, *72*, 924–930. [CrossRef] [PubMed]
17. Pozharitskaya, O.N.; Shikov, A.N.; Obluchinskaya, E.D.; Vuorela, H. The pharmacokinetics of fucoidan after topical application to rats. *Mar. Drugs* **2019**, *17*, 687. [CrossRef]
18. Barbosa, A.I.; Lima, S.A.C.; Yousef, I.; Reis, S. Evaluating the skin interactions and permeation of alginate/fucoidan hydrogels *per se* and associated with different essential oils. *Pharmaceutics* **2023**, *15*, 190. [CrossRef] [PubMed]
19. Bedoux, G.; Hardouin, K.; Burlot, A.S.; Bourgougnon, N. Bioactive components from seaweeds: Cosmetic applications and future development. *Adv. Bot. Res.* **2014**, *71*, 345–378.
20. Leelapornpisid, P.; Mungmai, L.; Sirithunyalug, B.; Jiranusornkul, S.; Peerapornpisal, Y. A novel moisturizer extracted from freshwater macroalga [*Rhizoclonium hieroglyphicum* (C.Agardh) K tzing] for skin care cosmetic. *Chiang Mai J. Sci.* **2014**, *41*, 1195–1207.
21. Wang, J.; Jin, W.; Hou, Y.; Niu, X.; Zhang, H.; Zhang, Q. Chemical composition and moisture-absorption/retention ability of polysaccharides extracted from five algae. *Int. J. Biol. Macromol.* **2013**, *57*, 26–29. [CrossRef] [PubMed]

22. Li, X.; Wu, N.; Chen, Y.; Tan, J.; Wang, J.; Geng, L.; Qin, Y.; Zhang, Q. Degradation of different molecular weight fucoidans and their inhibition of TGF-β1 induced epithelial-mesenchymal transition in mouse renal tubular epithelial cells. *Int. J. Biol. Macromol.* **2020**, *151*, 545–553. [CrossRef]
23. Mansour, M.B.; Balti, R.; Yacoubi, L.; Ollivier, V.; Chaubet, F.; Maaroufi, R.M. Primary structure and anticoagulant activity of fucoidan from the sea cucumber *Holothuria polii*. *Int. J. Biol. Macromol.* **2019**, *121*, 1145–1153. [CrossRef]
24. Chen, X.; Yang, S.; Wang, J.; Song, L.; Xing, R.; Liu, S.; Yu, H.; Li, P. Sulfated polysaccharides isolated from cloned *Grateloupia filicina* and their anticoagulant activity. *BioMed Res. Int.* **2015**, *2015*, 612352.
25. Bitter, T.; Muir, H.M. A modified uronic acid carbazole reaction. *Anal. Biochem.* **1962**, *4*, 330–334. [CrossRef]
26. DuBois, M.; Gilles, K.A.; Hamilton, J.K.; Rebers, P.A.; Smith, F. Colorimetric method for determination of sugars and related substances. *Anal. Chem.* **1956**, *28*, 350–356. [CrossRef]
27. Komatsu, H.; Takahata, T.; Tanaka, M.; Ishimitsu, S.; Okada, S. Determination of the molecular-weight distribution of low-molecular-weight heparins using high-performance gel permeation chromatography. *Biol. Pharm. Bull.* **1993**, *16*, 1189–1193. [CrossRef] [PubMed]
28. Yu-Hao, D.; Chun, C.; Xiong, F.; Rui-Hai, L. Study on the pharmacokinetics of mulberry fruit polysaccharides through fluorescence labeling. *Int. J. Biol. Macromol.* **2021**, *186*, 462–471. [CrossRef] [PubMed]
29. Tian, Q.; Quan, P.; Fang, L.; Xu, H.; Liu, C. A molecular mechanism investigation of the transdermal/topical absorption classification system on the basis of drug skin permeation and skin retention. *Int. J. Pharm.* **2021**, *608*, 121082. [CrossRef]
30. Barth, A. Infrared spectroscopy of proteins. *Biochim. Biophys. Acta* **2007**, *1767*, 1073–1101. [CrossRef]
31. Marty, J.P. NMF and cosmetology of cutaneous hydration. *Ann. Dermatol. Venereol.* **2002**, *129*, 131–136.
32. Rawlings, A.V.; Harding, C.R. Moisturization and skin barrier function. *Dermatol. Ther.* **2004**, *17*, 43–48. [CrossRef] [PubMed]
33. Ayala-Bravo, H.A.; Quintanar-Guerrero, D.; Naik, A.; Kalia, Y.N.; Cornejo-Bravo, J.M.; Ganem-Quintanar, A. Effects of sucrose oleate and sucrose laureate on in vivo human stratum corneum permeability. *Pharm. Res.* **2003**, *20*, 1267–1273. [CrossRef] [PubMed]
34. Anigbogu, A.N.C.; Williams, A.C.; Barry, B.W.; Edwards, H.G.M. Fourier transform raman spectroscopy of interactions between the penetration enhancer dimethyl sulfoxide and human stratum corneum. *Int. J. Pharm.* **1995**, *125*, 265–282. [CrossRef]
35. Godin, B.; Touitou, E. Transdermal skin delivery: Predictions for humans from in vivo, ex vivo and animal models. *Adv. Drug Deliv. Rev.* **2007**, *59*, 1152–1161. [CrossRef]
36. Jacobi, U.; Kaiser, M.; Toll, R.; Mangelsdorf, S.; Audring, H.; Otberg, N.; Sterry, W.; Lademann, J. Porcine ear skin: An in vitro model for human skin. *Ski. Res. Technol.* **2007**, *13*, 19–24.
37. Farwick, M.; Lersch, P.; Strutz, G. Low molecular weight hyaluronic acid: Its effects on epidermal gene expression & skin ageing. *SOFW J.* **2008**, *134*, 1–8.
38. Knorr, F.; Lademann, J.; Patzelt, A.; Sterry, W.; Blume-Peytavi, U.; Vogt, A. Follicular transport route-research progress and future perspectives. *Eur. J. Pharm. Biopharm.* **2009**, *71*, 173–180.
39. Zhang, S.; Song, W.; Wu, H.; Wang, J.; Wang, Y.; Zhang, Z.; Lv, H. Lecithins-Zein nanoparticles for antifungal treatment: Enhancement and prolongation of drug retention in skin with reduced toxicity. *Int. J. Pharm.* **2020**, *590*, 119894. [CrossRef]
40. Fartasch, M.; Bassukas, I.D.; Diepgkn, T.L. Structural relationship between epidermal lipid lamellae, lamellar bodies and desmosomes in human epidermis: An ultrastructural study. *Br. J. Dermatol.* **1993**, *128*, 1–9. [CrossRef]
41. Ren, Y.H.; Zhou, Q.; Xu, Y.; Xu, B.N.; Shu, P.; Peng, L.H. Casting new light on the retinol and retinyl palmitate functions as chemical enhancers for transdermal/topical drug delivery. *Adv. Healthc. Mater.* **2025**, *14*, e2402836. [CrossRef]
42. Ren, Y.; Li, Z.; Xu, Y.; Ding, Y.; Song, Q.; Hu, Y.-J.; Peng, L. Harnessing Flavonoids for Transdermal Enhancement: Sustainable Strategies to Improve the Permeability of Hydrophilic Drugs through the Transformation of Keratins and Lipids. *ACS Sustain. Chem. Eng.* **2025**, *13*, 6433–6450. [CrossRef]
43. Triantafyllopoulou, E.; Pippa, N.; Demetzos, C. Protein-liposome interactions: The impact of surface charge and fluidisation effect on protein binding. *J. Liposome Res.* **2023**, *33*, 77–88.
44. Tang, Z.; Guo, X.; Wen, X.; Wang, Y.; Lu, H. Effects of hyaluronic acid with different relative molecular weights on the transdermal absorption of reduced glutathione. *J. China Pharm. Univ.* **2021**, *52*, 203–210.
45. Ni, C.; Liao, Q.; Ying, R.; Hayat, K.; Salamatullah, A.M.; Huang, M. Recent advances in surface-modified liposomes with polysaccharides for bioactive delivery. *Food Chem.* **2025**, *492*, 145580. [CrossRef] [PubMed]
46. Valachová, K.; Šoltés, L. Self-associating polymers chitosan and hyaluronan for constructing composite membranes as skin-wound dressings carrying therapeutics. *Molecules* **2021**, *26*, 2535. [CrossRef]